LANGMUIR Article
Cite This: Langmuir 2019, 35, 7312−7321
pubs.acs.org/Langmuir

Correlation of Surface Morphology and Interfacial Adhesive Behavior between Cellulose Surfaces: Quantitative Measurements in Peak-Force Mode with the Colloidal Probe Technique

Yuli Lai,[†,∥] Hao Zhang,[‡,∥] Yasuhito Sugano,[§] Hui Xie,[*,‡] and Pasi Kallio[*,†]

[†]Micro- and Nanosystems Research Group, Faculty of Medicine and Health Technology, Tampere University, P.O. Box 692, 33101 Tampere, Finland

[‡]The State Key Laboratory of Robotics and Systems, Harbin Institute of Technology, Harbin 150080, PR China

[§]Department of Industrial Chemistry, Faculty of Engineering, Tokyo University of Science, 1-3 Kagurazaka, Sinjuku-ku, Tokyo 162-8601, Japan

ABSTRACT: A better understanding of cellulose−cellulose interactions is needed in applications such as paper making and all-cellulose composites. To date, cellulose−cellulose studies have been chemistry-oriented. In these studies, the sample surfaces have been modified with different chemicals and then tested under an atomic force microscope (AFM) using a colloidal probe (CP). Studies of cellulose−cellulose interaction based on sample morphology and mechanical properties have been rare as a result of the complex surface structure and the soft texture of the cellulose. The current surface interaction models, such as the Johnson−Kendall−Roberts (JKR) model in which the studied bodies are assumed to have smooth surfaces, can no longer fully reveal the interfacial behavior between two cellulose surfaces. Therefore, we propose a new type of contact model for rough−rough interaction by dividing the surface contacts into primary and secondary levels. The main idea of the new model is to take into account local individual contact details between rough surfaces. The model considers the effect of the surface topography by including the asperities and valleys on a cellulose sphere used as the colloidal probe in imaging the topography of a cellulose membrane (CM). In addition, the correlation between the surface morphology and adhesion is studied. To verify the importance of including the effect of the surface roughness in contact analysis and validate our hypothesis on the correlation between the surface morphology and adhesion, an extensive set of experiments was performed. In the experiments, a combination of the AFM peak-force mode (PFM) and the CP technique was employed to acquire a massive amount of information on cellulose−cellulose interactions by measuring the adhesion among six CSs of different sizes and a CM.

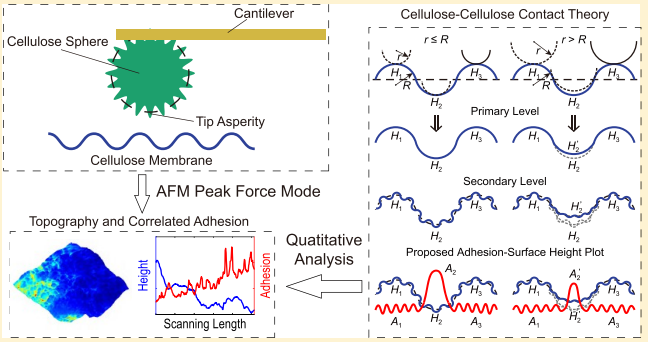

INTRODUCTION

Cellulose, as the most abundant polymer in plants and trees, is used as a raw material, for example, in paper, biocomposite, and textile products.[1] In these various products involving cellulose, the interfacial interactions are of particular interest because they influence not only the mechanical properties of the product but also its production. By means of paper products, their mechanical properties depend as much on the network structure and the bond strength between cellulose fibers as on the single cellulose fiber strength. The importance of the interface was also emphasized in a recent review[2] on all-cellulose composites in which the authors concluded that further insights into the interfacial phenomena between cellulosic surfaces are needed to fully utilize the benefits and potential of monocomponent composites.

Natural cellulose fibers (NCFs) are porous microscale objects. Unlike most artificial fibers, such as glass fibers, which have a unified shape and a smooth surface, each NCF has a unique shape with a rough surface. These characteristics make it very difficult to directly measure the cellulose surfaces' interactions using individual NCFs for two reasons. First, the random shape of NCF is a significant obstacle for sample positioning and grasping during the measurement operation; second, the porous and rough surface leads to an inaccurate estimation of the interfacial contact area, which is later required to normalize the force result. Therefore, this study employs the technique of colloidal probe (CP) atomic force microscopy (AFM), which was introduced by Butt and Ducker et al.[3,4] for interaction measurements. In the CP technique, either a tip of an AFM probe is modified to a semispherical shape or a single spherical colloid is glued to a tipless AFM probe cantilever.[5] Because the NCF is a cellulose-based

Received: October 17, 2018
Revised: May 2, 2019
Published: May 7, 2019

DOI: 10.1021/acs.langmuir.8b03503
Langmuir 2019, 35, 7312−7321

Table 1. Catalog of Cellulose Adhesion Research[a]

material	contact mode	measured force	technique	surface treatment	environment	adhesion and surface morphology correlation	refs
c−c	s−p	interaction	scanning probe	yes	aqueous	no	1
c−c	s−p	friction		yes	aqueous	no	6
c−o	s−p	interaction	pull-off	no	aqueous	no	7, 26
c−c	s−p	interaction	pull-off	yes	aqueous	no	8, 13, 24
c−c	s−s	interaction	scanning probe	no	air and aqueous	no	14
c−c	s−s	interaction	pull-off	no	aqueous	no	15
c−c	s−p	friction		no	air	no	16
c−c	s−s	friction		no	aqueous	no	17
c−o	s−p	interaction	pull-off	no	air	no	18, 25
c−c	s−p	interaction (adhesion)	peak force	no	air	yes	our study

[a]Cellulose−cellulose, c−c; cellulose−other material, c−o; sphere−sphere, s−s; sphere−plane, s−p.

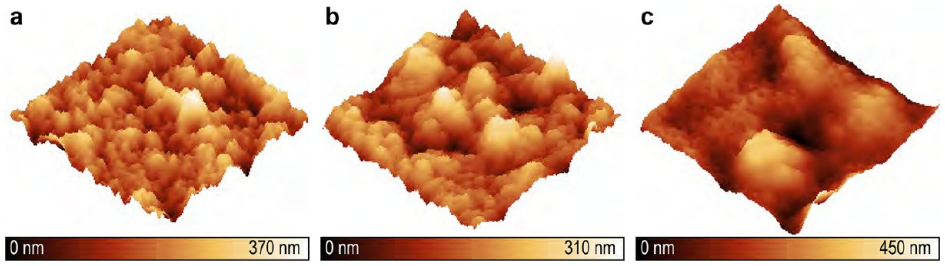

Figure 1. Cellulose membrane topography obtained by applying (a) a normal AFM probe, (b) CP with a 2.5 μm CS ,and (c) CP with a 2.5 μm BS. Scan area: 15 μm × 15 μm.

material, cellulose microspheres (CS) are selected to mimic NCF in the measurements. Compared to the measurement of interactions between individual NCFs, the CP technique is more reliable and convenient to employ as the cellulose CP can be pushed against a cellulose substrate to obtain the force data. So far, this technique has been widely adopted in interaction force studies of cellulose-based materials[1,6−18] as well as many other materials.[3,4,19−22]

Nowadays, the most common method used for measuring interaction forces between different material surfaces involves employing the CP technique under normal AFM working modes, such as the pull-off mode (POM)[7,8,13,18,23−27] and the force volume mode (FVM).[27−29] These techniques collect single force curves or an array of force curves, which are plots of force as a function of the probe displacement along the axis perpendicular to the surface (z axis). Obtaining an adhesion map requires acquiring adhesion data from thousands of force curves. Therefore, it takes several hours to complete the process because each force curve generally takes approximately 1 s to collect. In addition, environmental scanning electron microscopy (ESEM), which is known for its precise control of environmental conditions (e.g., humidity, temperature),[30] is also used to measure interaction forces, especially the adhesion between cell substrates.[31,32] However, ESEM is not suitable for making quantitative data measurements in batches.

Nevertheless, the newly developed peak-force mode (PFM) reduces the whole mapping process to several minutes by acquiring the force curves at high speed with high precision force control.[33] Moreover, when using the PFM, it is possible to correlate the adhesion with the substrate morphology because the PFM can acquire substrate topography images of fairly high resolution synchronously with the force data, which cannot be done by using the POM or FVM. Therefore, on the basis of the aforementioned facts, we propose to use the CP technique with the PFM (CP-PFM) for the cellulose−cellulose interaction study.

In many of the previous cellulose-related force studies (shown in Table 1), the measurements were conducted in aqueous solution or using surface-treated/coated cellulose materials. Different from the previous studies, we use pure cellulose without any surface treatment or coating, and the measurements are carried out in air. The main purpose of this study is to create a new model of rough−rough surface interaction and correlate the adhesion to the morphology of the sample substrate. To the best of our knowledge, this is the first paper to use the CP-PFM technique for such a purpose in cellulose research.

In this article, CSs of different sizes were selected to prepare the CPs for adhesion measurements. Quatitative measurements were performed between each cellulose CP and a pure cellulose membrane (CM). A customized dual-probe AFM was programmed and employed to complete the preparation of the CP and conduct the PFM for high-speed measurements of interaction properties. The extensive quantity of data obtained in this article provides an opportunity to connect the adhesive behavior between cellulose surfaces based on their morphology with statistically higher reliability, which previous studies have not done because of limitations in the available techniques.

THEORETICAL ASSUMPTION AND MODELING

Effect of Tip Asperities. It is known that the quality of an obtained topography image depends largely on the morphology of the probe tip employed for scanning.[34] According to the tip-broadening effect, an AFM probe with a smaller tip reveals more precise information about the surface properties and produces images with features much closer to the real topography of the sample than using a probe with a larger tip. Therefore, the topography images obtained by two CPs having the same size should have approximately the same

DOI: 10.1021/acs.langmuir.8b03503
Langmuir 2019, 35, 7312−7321

number of feature details and differ largely from the images acquired with a standard AFM tip.

However, when compared to the topography images obtained using a borosilicate sphere (BS) tip, the topography provided by a CS tip reveals more details and information and is similar in quality to images scanned by a standard AFM tip (Figure 1). This observation suggests that the interaction behavior measured with a rough-surface CS is governed by the tiny asperities on the surface of the CS (Figure 2). Figure 3

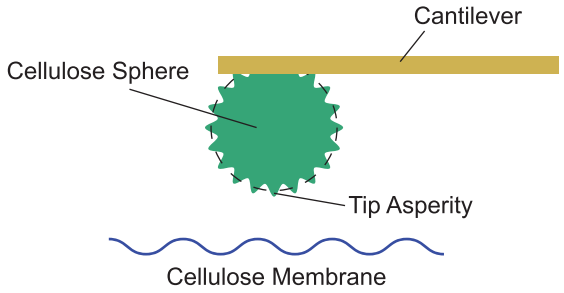

Figure 2. Tip asperities.

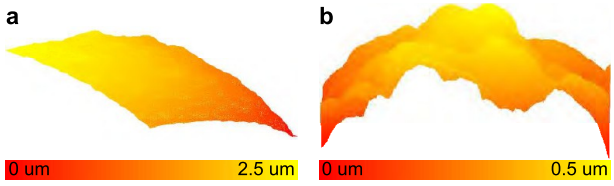

Figure 3. Three dimensional topography of the BS (a) and CS (b) tips. Scan area: 2 μm × 2 μm.

demonstrates AFM images of the BS (a) and CS (b) tips. The substantial difference between these two tips is the asperities which are found on the CS surface, whereas the BS surface is significantly smoother. Therefore, it is reasonable to believe that more information and geometrical details can be obtained by using a CS-based CP instead of a CP that has a smooth surface similar to BS.

Contact Model. In a previous research paper,[35] Kumar et al. established a model between a smooth sphere and a substrate with a rough surface, where the morphology of the substrate surface was simplified and represented by primary and secondary asperities and valleys. In our case, there are primary and secondary asperities and valleys in both the CS and CM because they both have rough surfaces. In addition, so far the most commonly used model for demonstrating the interaction between two surfaces is the Johnson–Kendall–Roberts (JKR) model. The JKR model is applied normally on smooth–smooth surface contact and it is an equilibrium model, which cannot accurately describe the interaction of a rough–rough surface with a short contact time of less than 1 s. However, it is still efficient to use the JKR to estimate the adhesion value at each contact spot and predict the adhesion dynamics as a function of CS size when analyzing the contact surfaces that are fragmentary at primary and secondary levels.

At the primary level, there are two scenarios in terms of the contact relationship for a sphere and a substrate: the sphere interacts either with the primary asperity (Figure 4a) or with the primary valley (Figure 4b,c) on the substrate. When the sphere is in contact with the primary asperity of the substrate, the adhesion between them can be calculated with eq 1. When the interaction occurs between the sphere and the primary

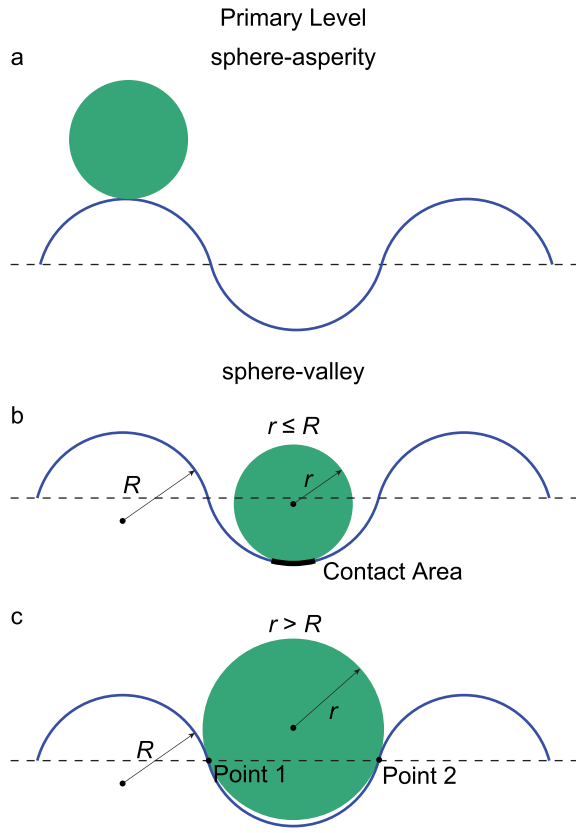

Figure 4. Contact modes between CS and CM at the primary level: (a) sphere–asperity contact, (b) sphere–valley contact when $r \leq R$, and (c) sphere–valley contact when $r > R$.

valley, the adhesion can be estimated using eq 2 (if sphere radius $r \leq$ primary asperity/valley radius R) and eq 3 (if $r > R$). On the basis of these equations, the adhesion should always increase when the size of the sphere increases. However, there is a possible decrement in adhesion at the turning point when r becomes larger than R as a result of the decreasing contact area.

$$F_{pa} = \frac{3}{2}\pi W\frac{rR}{r+R} \tag{1}$$

$$F_{pvs} \geq \frac{3}{2}\pi Wr \tag{2}$$

$$F_{pvl} = F_1 + F_2 = 2 \times \frac{3}{2}\pi W\frac{rR}{r+R} = 3\pi W\frac{rR}{r+R} \tag{3}$$

It is easy to conclude

$$F_{pa} < F_{pv} \tag{4}$$

In eqs 1–4, W is the work of separating the contact surfaces, F_{pa} is the primary asperity–asperity adhesion force, F_{pvs} is the primary asperity–valley adhesion when $r \leq R$, F_{pvl} is the primary asperity–valley adhesion when $r > R$, F_1 and F_2 are adhesion at points 1 and 2, respectively, and F_{pv} is the primary asperity–valley adhesion force in general.

At the secondary level, the interactions are caused by the surface roughness of the sphere and the substrate. Similar to the primary level, there are also two contact scenarios: asperity–asperity and asperity–valley, as shown in Figure 5. When the influences from the primary asperities and valleys are

DOI: 10.1021/acs.langmuir.8b03503
Langmuir 2019, 35, 7312–7321

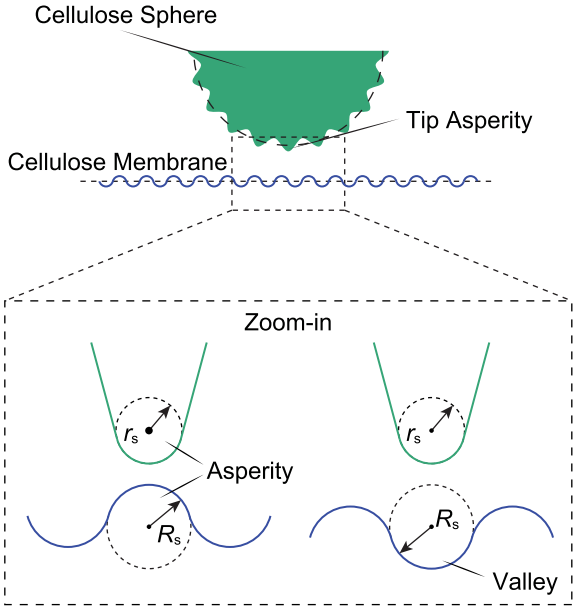

Figure 5. Contact modes between CS and CM at the secondary level. (Left) Asperity−asperity contact. (Right) Asperity−valley contact.

neglected, the secondary asperity−asperity adhesion can be expressed as eq 5. The secondary asperity−valley adhesion can be demonstrated by eq 6 or 7.

$$F_{sa} = \frac{3}{2}\pi W\frac{r_s R_s}{r_s + R_s} \tag{5}$$

$$F_{svs} \geq \frac{3}{2}\pi W r_s \tag{6}$$

$$F_{svl} = 3\pi W\frac{r_s R_s}{r_s + R_s} \tag{7}$$

Then it is obvious that

$$F_{sa} < F_{sv} \tag{8}$$

In eqs 5−8, r_s and R_s are the equivalent radii of the secondary tip asperity and the secondary substrate asperity/valley, respectively. F_{sa} is the secondary asperity−asperity adhesion force, F_{svs} is the secondary asperity−valley adhesion when $r_s \leq R_s$, F_{svl} is the secondary asperity−valley adhesion when $r_s > R_s$, and F_{sv} is the secondary asperity−valley adhesion force in general.

On the basis of these equations, it is easy to deduce that the CP experiences a higher adhesion force on valleys than on asperities at both primary and secondary levels. This is different from the case in ref 35 where no adhesive interactions occurred in the secondary valleys of the substrate surface because the sphere surface was considered to be smooth.

Theoretical Scanning Model and Surface Height−Adhesion Plots. According to the contact model provided above, when a CP is employed to conduct the topography scanning, the output of the measurements should follow the patterns shown in Figure 6. At the primary level, only when the radius of the CP is no larger than the radius of the primary valley, the CP can reach the bottom point H_2 of the surface primary valley. Otherwise, the CP cannot come into contact with the bottom of the valley. In this case, the surface height value acquired by the AFM system is H_2' instead of the actual

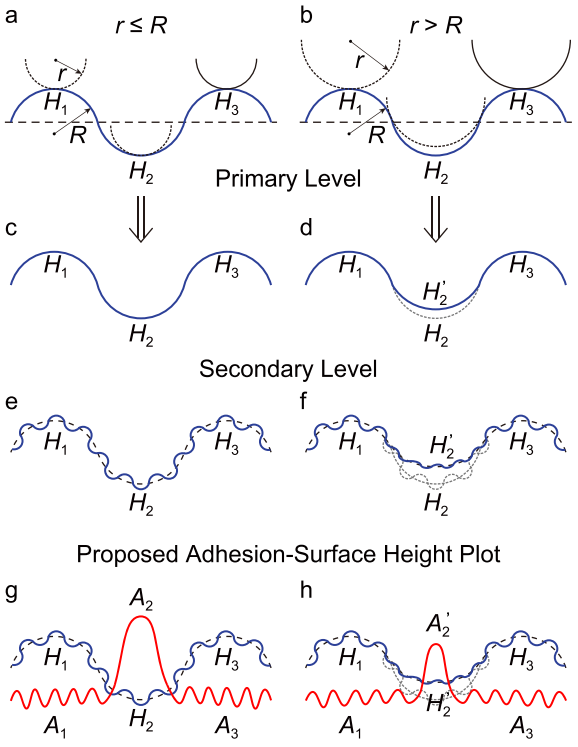

Figure 6. Scanning patterns and adhesion−surface height plots for CS−CM. (a and b) General contact patterns between probe and substrate; (c and d) scanning pattern at the primary level; (e and f) scanning pattern at the secondary level; (g and h) proposed adhesion−surface height plot. (a, c, e, and g) Patterns and plots when $r \leq R$. (b, d, f, and h) Patterns and plots when $r > R$.

height H_2 because of the tip size effect. At the secondary level, it is extremely difficult to predict the actual scanning pattern because there can be multiple tip asperities in contact with the substrate surface at the same time. However, an approximation of the pattern can be drawn as presented in Figure 6e,f. Additionally, it is already known from the contact model that the adhesion is always higher in surface valleys at both primary and secondary levels for rough−rough surface interaction. Therefore, it is reasonable to describe the surface height−adhesion plots as those in Figure 6g,h, where the adhesion force experiences peak values at valleys.

EXPERIMENTAL SECTION

Materials. The adhesion force among six CSs of different sizes and pure (100%) CMs was measured using the CP technique in the PFM. To make the CM, dry cellulose (Sigma-Aldrich) was added and dissolved in 1.3 M NaOH solution. The mixture was then dropcast onto a glass surface. Afterward, the sample was left to dry before being immersed in a H_2SO_4 bath. Finally, an excess amount of deionized (DI) water was used to wash the regenerated samples before they were stored in water for later use. Using such a fabrication method, CM should have no other components other than cellulose.

Nonchemically treated CSs (CELLULOBEADS D-10 and D-30) were provided by KOBO. Six standard AFM probes (HQ: NSC18/Al BS, Mikromash) with a spring constant of 2.8 N/m were modified with a focused ion beam (FIB) to remove the tips for CP preparation. A customized dual-probe AFM system[36] was employed to prepare the CP and measure the adhesion force between the CSs and CM. More details are given, along with a description of the system setup, in the following paragraphs.

Experimental Setup. As shown in Figure 7, this system consists of two probe holders (PH I and PH II), which are installed on two 3-

DOI: 10.1021/acs.langmuir.8b03503
Langmuir 2019, 35, 7312−7321

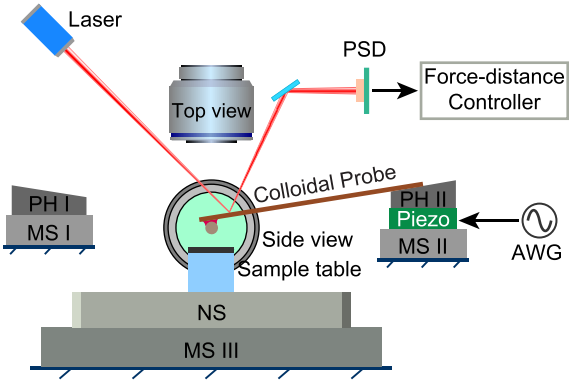

Figure 7. Setup scheme of the customized dual-probe AFM system.

DOF micropositioning stages (MS I and MS II), an optical lever system with a laser and a position-sensitive detector (PSD), and two optical microscopy systems (top view and side view). The sample table is fixed on a 3-DOF nanopositioning stage (NS) located on a 3-DOF micropositioning stage (MS III). The colloidal probe can be made by simultaneously manipulating MS I and MS II under the two optical microscopy systems. (More details are given in the next section.) During the measurement, an arbitrary waveform generator (AWG) is used to drive a piezoelectric actuator of PH II to realize the periodic motion of the probe used in the PFM scanning. The cantilever deflection is measured with the PSD and fed to the force–distance (FD) controller, which controls the maximum force between the probe and the sample and also records the adhesion force between them using a reference force value. The maximum force applied to the probe is referred to as the peak force, and the adhesion force is equal to the force at which the probe detached from the sample.

Preparation of the Colloidal Probe. First, the CS samples were placed into an acetone bath, followed by washing with an excess amount of DI water several times before being dried in an oven at 60 °C for 12 h. After the CS samples were ready, they were transferred onto a clean cover glass, which was mounted on the sample table.[37,38] A selected CS was picked up by applying negative pressure through a microcapillary. When the CS picking was completed, the microcapillary was removed from PH I under negative pressure while still holding the CS on its head and carefully suspending it in a Petri dish. Then, a thin tungsten wire, cast with a small droplet of epoxy resin glue (ergo 7200), as well as the aforementioned standard AFM probe, were mounted on PH I and PH II, respectively. A tiny amount of glue was transferred from the wire to the front of the AFM cantilever surface by adjusting the positions of the PH I. After the drop of glue was deposited onto the AMF cantilever, the tungsten wire was removed and the microcapillary with the chosen CS was remounted onto PH I. The CP preparation was completed by moving the CS on the microcapillary tip onto the AFM cantilever surface and approaching the drop of glue until a part of the sphere was merged with the glue, thereby guaranteeing a rigid connection between the probe and the sphere. After 24 h, the customized AFM colloidal probe was ready, given that the glue was completely solidified. The process is depicted in Figure 8.

The Cleveland method[39] was used to calibrate the spring constant of the prepared CPs. This method requires measuring the resonance frequencies of the CP before and after adding a known mass to the end of the cantilever. (In our case, this mass was a tin sphere with a radius of 20 μm.) As a result, the real spring constant can be calculated from the measurement data. The CS diameters were measured in a scanning electron microscope (SEM), shown in Figure 9. Subsequently, the CS radius and the actual spring constants of the CPs are presented in Table 2.

The prepared CP was then used to measure the adhesion force between the CS and the CM. Quantitative (256 × 256) measurements were conducted for each CS sample by applying the PFM in the customized AFM setup. In the PFM, a sinusoidal signal is given to

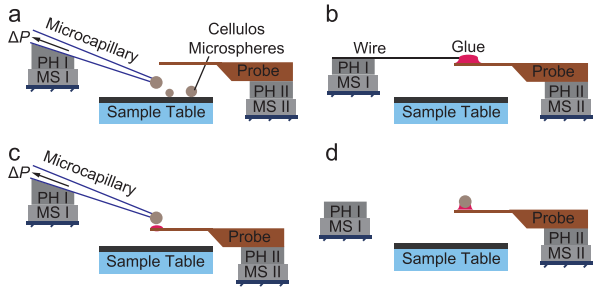

Figure 8. Preparation of the colloidal probe. (a) Picking the chosen CS with a microcapillary. (b) Depositing glue onto the AFM probe. (c) Gluing the chosen CS onto the AFM probe. (d) Schematic of the finalized colloidal probe.

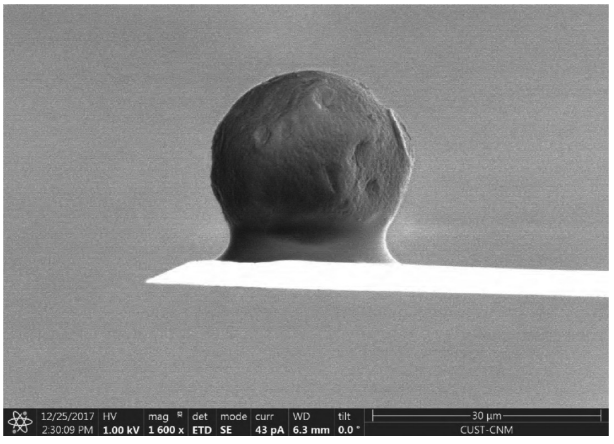

Figure 9. SEM image of the CP with CS.

Table 2. Calibrated Actual Spring Constants of Prepared CPs with Different CS Sizes

tip	CS_1	CS_2	CS_3	CS_4	CS_5	CS_6
CS radius (μm)	3.3	5.3	7.48	13.18	14.35	16.54
actual spring constant (N/m)	1.92	2.35	2.07	2.51	1.50	2.21

provide a vertical oscillation so that the CP is driven to approach and retract the sample surface repeatedly at high frequency. Meanwhile, the responding force curves are recorded by the FD controller system as the output of the interaction between the CP and the CM. Each force curve represents one test cycle including the peak force and the adhesion force as illustrated in Figure 10. The adhesion, referred as the pull-off which is the lowest point of the force curve, is obtained by means of a conventional lowest point search. In our tests, the peak force was set to 15 nN. The number of sampling points for each force curve was 1000, and the scan rate was 1 line/s. The oscillation

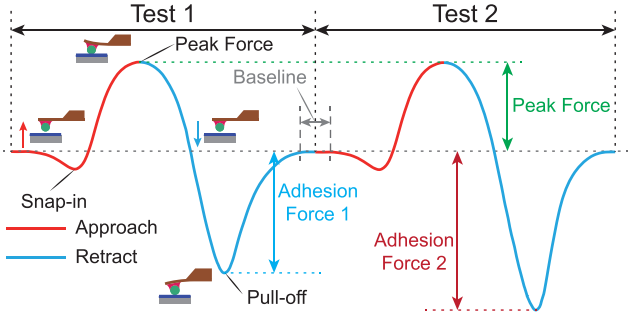

Figure 10. Adhesion data acquisition principle.

DOI: 10.1021/acs.langmuir.8b03503
Langmuir 2019, 35, 7312−7321

frequency of the probe was kept constant at 1 kHz, whereas the oscillation amplitude was different for each CS−CM pair. The main idea is to keep the amplitude larger than the value of the adhesion force/probe stiffness such that the adhesion value can be correctly detected. In these tests, the oscillation amplitude was between 20 and 30 nm. The obtained topography and adhesion images have a resolution of 256 pixels × 256 pixels (step size, 10 nm). Temperature and humidity were controlled to 23 ± 1 °C and 14 ± 1%, respectively, in order to prevent unnecessary disturbances from the environment.

Surface Homogeneity. The adhesion value depends largely on the surface energy and morphology of the sample. When the sample has a homogeneous surface, the adhesion values between the sample and the same probe should be similar at different locations on the sample surface and vice versa. The adhesion histograms (Figure 11)

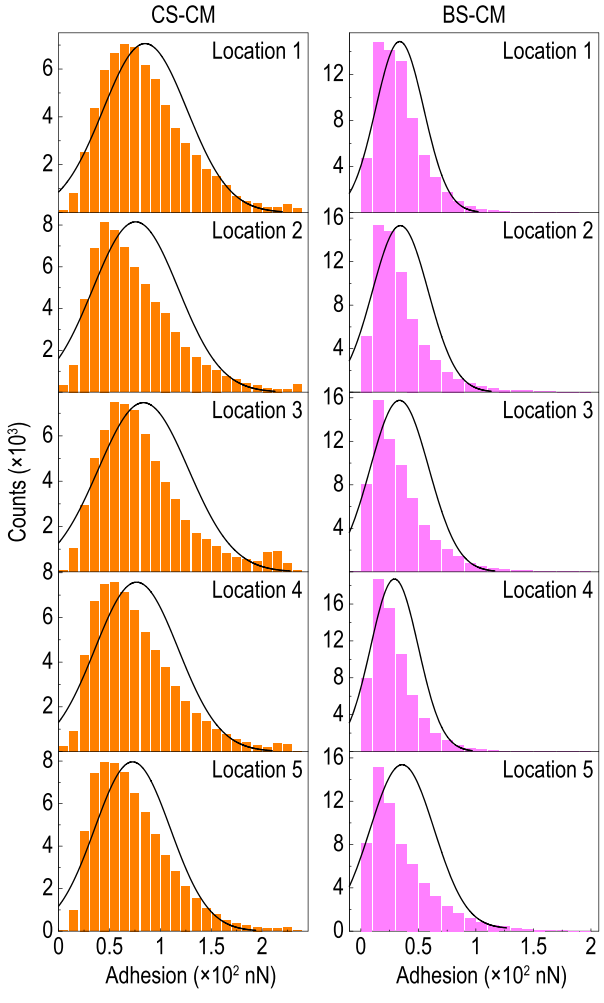

Figure 11. Adhesion histograms and Gaussian fit curves of CS−CM and BS−CM at five different locations.

and statistical data (Table 3) of the CS−CM and the BS−CM (CS radii, 2.5 μm; BS radii, 2.5 μm) reveal the similarity of the adhesion distributions at five random locations on the CM sample, which indicates the homogeneity of the sample surface. Therefore, the adhesion difference should be small for the same CS probe at different locations on the CM sample.

Table 3. Mean and Standard Deviation for the Adhesion of CS−CM and BS−CM at Different Locations

location	1	2	3	4	5
CS−CM (nN)	84.98	75.66	83.31	76.63	72.62
standard deviation (nN)	41.40	42.06	44.31	40.91	37.16
BS−CM (nN)	33.77	34.31	33.62	29.23	35.85
standard deviation (nN)	20.94	24.28	25.43	20.73	27.86

RESULTS AND DISCUSSION

Comparison to the Johnson−Kendall−Roberts Model. The adhesion force of six CS−CM pairs were obtained by using PFM, which returned an excessively large amount of data for plotting adhesion histogram for each sample pair as shown in Figure 12a−f. Table 4 presents both

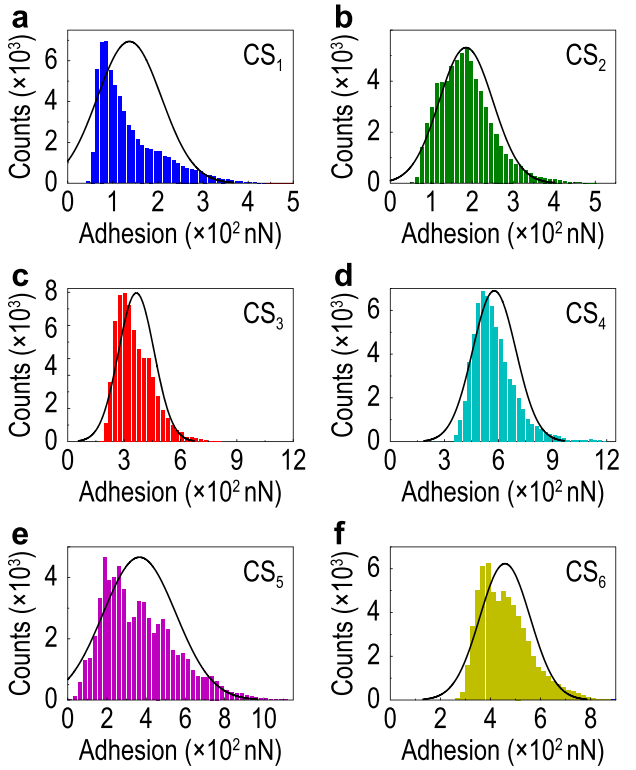

Figure 12. Adhesion histograms and Gaussian fit curves of CS_1−CS_6: (a−f).

the experimental and theoretical adhesion forces for each CS−CM pair, where the theoretical values were calculated from the JKR model using eq 9. Subsequently, all of these data were

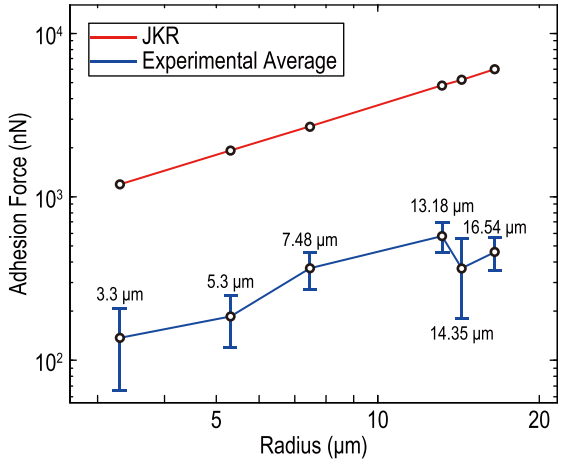

Figure 13. Experimental and JKR adhesion forces.

DOI: 10.1021/acs.langmuir.8b03503
Langmuir 2019, 35, 7312−7321

Table 4. Experimental and JKR Model Calculated Adhesion Forces of Differently Sized CSs

tip	CS_1	CS_2	CS_3	CS_4	CS_5	CS_6
experimental adhesion force (average) (nN)	136.79	184.78	365.11	576.61	365.93	457.72
standard deviation (nN)	70.95	65.55	94.80	119.93	185.58	100.54
JKR adhesion force (nN)	1197.4	1923.1	2714.1	4782.4	5207.0	6001.6

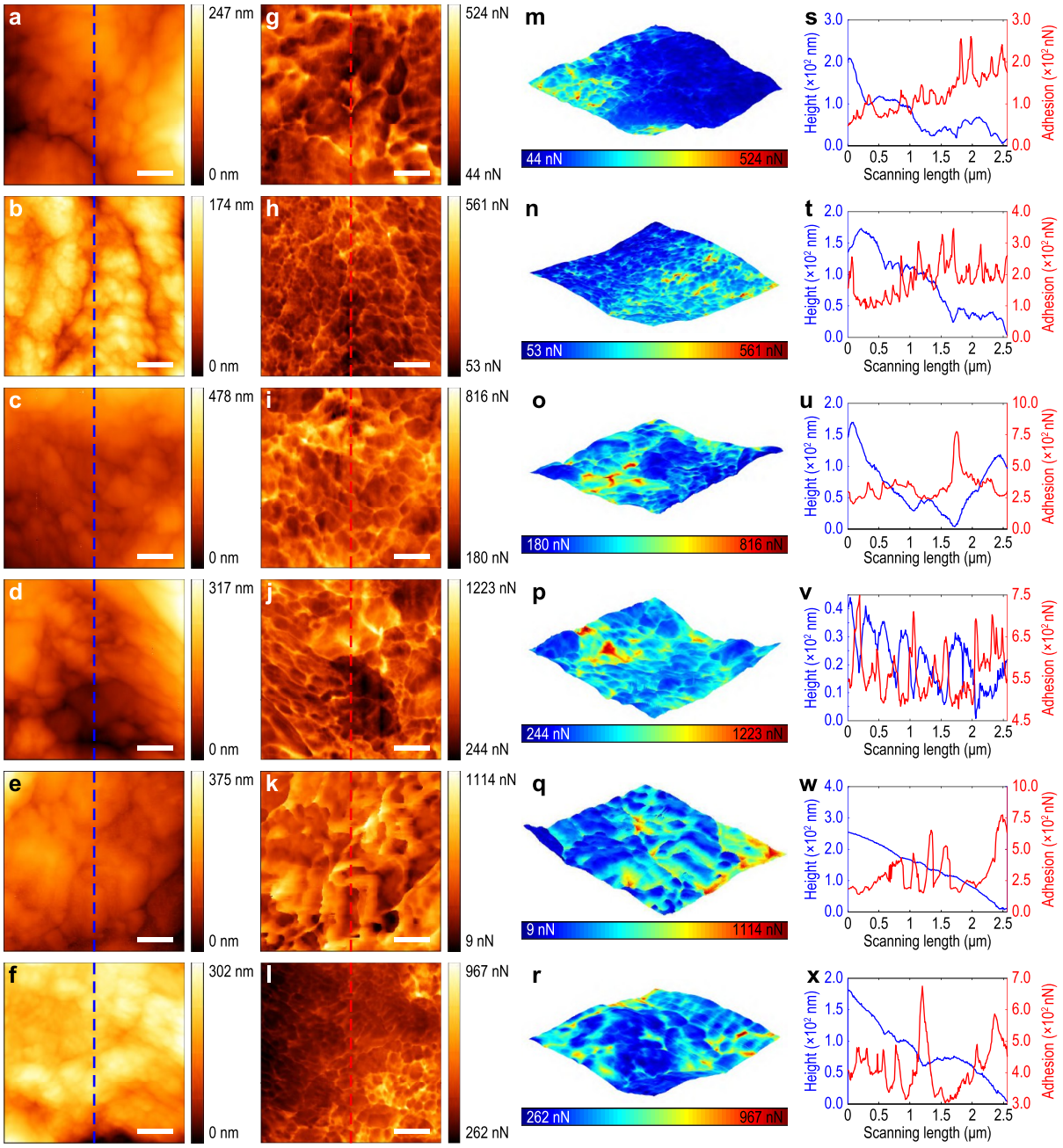

Figure 14. Measurements conducted among CS_1, CS_2, CS_3, CS_4, CS_5, CS_6, and CM: (a–f) topography, (g–l) adhesion map, (m–r) four-dimensional images combining the three-dimensional topography with the adhesion (color bar), (s–x) and the correlated surface height and adhesion comparison plots. The minimum height is fixed to zero in s–x. Scale bar in a–l: 500 nm.

plotted in the same figure (Figure 13) to facilitate the comparison. Compared with the JKR model, where the adhesion force constantly increases with an increase in the sphere radius, the increasing trend for the measured adhesion force is interrupted after the sphere radius reaches 13.18 μm. The reasonable explanation for this phenomenon is that the size of CS at this point becomes comparable to the size of the primary valleys on CM. Consequently, the average contact area between the CS and CM reaches an interim maximum level. As a result, the adhesion force is maximized at this moment. Once the size of CS becomes higher (at 14.35 μm) than the primary valleys, the adhesion force drops from the previous maximum point (at 13.18 μm) and starts to increase again as the size of the CS increases (from 14.35 to 16.54 μm).

DOI: 10.1021/acs.langmuir.8b03503
Langmuir 2019, 35, 7312–7321

$$F_{JKR} = \frac{3}{2}\pi r_{cs} 2\sqrt{\gamma_{cs}\gamma_{cm}} \quad (9)$$

γ_{cs} is the surface energy of CS, γ_{cm} is the surface energy of CM, and r_{cs} is the radius of CS. The surface energy of untreated cellulose (38.5 mJ/m^2[40]) is used in eq 9 to replace the values of γ_{cs} and γ_{cm} because CS and CM are untreated pure cellulose samples.

Moreover, the theoretical adhesion forces produced by the JKR model have much higher values than the experimental adhesion forces. The JKR model is known as an equilibrium theory. In PFM experiments, the contact time between the CP and the sample surface is <1 ms, which is much shorter than the time needed to achieve an equilibrium. Nordgren et al.[41] have studied the relationship between the contact time and the work of adhesion between a PCL-grafted cellulose sphere and a neat cellulose sphere (both having a diameter of 10−15 μm). According to their study, the work of adhesion as a function of the contact time increases from about 12 fJ with short contact times to about 20 fJ at long contact times at a temperature of 20 °C. The work of adhesion increases slowly and steadily from the initial point to the equilibrium point. Therefore, we suggest that there will be an increase in the adhesion force if we increase the contact time. However, extending the contact time to the equilibrium level should only increase the adhesion value to be not more than the theoretical value that was calculated from the JKR model. As mentioned in the previous section, this article focuses on creating a new contact model for interactions between rough surfaces and also correlating the adhesion to the local morphology of the sample surface. Although increasing the contact time at a certain location can increase the adhesion at this particular location, the correlation of adhesion−surface morphology should still follow the same patterns (Figure 6g,h) as long as the contact time is kept the same for each test location of the sample surface. The PFM is known for its precise control of the maximum applied force, thus when the sample surface is homogeneous, which has been proven in the previous section, the contact time should remain constant throughout the tests. Therefore, we believe that using the CP-PFM can still provide fairly accurate adhesion variation trends, regardless of the short contact time between the two cellulose surfaces.

The purpose of comparing experimental values in this study with the JKR model is to reveal the role of the CS size and the surface morphology of the sample on adhesion variations. The adhesion calculated from the JKR model increases as the size of the CS increases, but in real experiments, this is not necessarily the case. CS_5 and CS_6 have larger radii than CS_4, but the measured adhesion is larger on CS_4 than on CS_5 and CS_6. Thus, the JKR model is not descriptive in the case in which the contact surfaces are rough.

Adhesion Force and Surface Morphology. The Effect of Tip Asperities subsection proved that the topography and the adhesion images obtained by the CS probe are informative. This means that the synchronously obtained sample adhesion maps and topographies can reveal the effects of surface morphology on adhesion forces when correlating these two types of images. To facilitate image analysis, four-dimensional images were assembled by adding the adhesion forces as an extra dimension to the original three-dimensional topography image (Figure 14a−f). Additionally, the surface height values were extracted from the topography data and paired with the adhesion force values for the same locations along the selected scanning line (as marked with dotted lines in Figure 14a−l). Subsequently, the surface height and correlated adhesion are presented together as shown in Figure 14s−x, from which it can be observed that the adhesion force peaks frequently appear at primary and secondary valleys on the surface; this resembles the description in the modeling part.

To investigate the numerical relationship of adhesion and surface height, the normalized adhesion (F_{adh}/r) as a function of surface depth ($H_{max} - H$, the difference between the highest height and the local height of the scanned surface) is plotted in Figure 15 by extracting the data from the adhesion−surface height plots of Figure 14s−x. Then the scattered data are polynomial fitted with a smooth curve. In general, the curve shows that the obvious increase in adhesion occurs at a surface depth of >100 nm. At depths below this value, there is no significant change in the adhesion. However, when analyzing the scattered data set for each CS individually, it was noticed that the patterns of CS_1, CS_2, CS_3, CS_5, and CS_6 are similar; meanwhile, the pattern of CS_4 differs a lot from those of the other ones. As mentioned, one possible reason for this phenomenon is that the radius of CS_4 is comparable to the primary asperity/valley radius (R) of the CM surface. In this case, the contact area can be maximized when CS_4 interacts with the CM sample surface. As a result, the normalized adhesion of CS_4−CM is higher than that of the other CS−CM pairs at the same surface depth levels as shown in Figure 15.

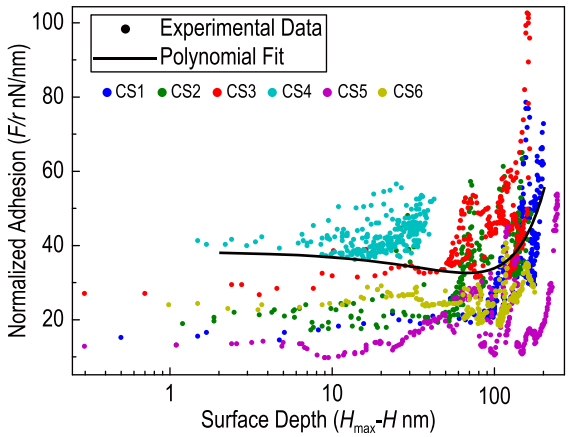

Figure 15. Normalized adhesion as a function of surface depth for CS_1−CS_6.

CONCLUSIONS

In the present study, a novel contact model was proposed to correlate the adhesion force and the surface morphology by including the primary and secondary level morphology both in the cellulose sphere (CS) and cellulose membrane (CM) surface. The effect of the tip asperity was introduced and verified through comparing the membrane topographies obtained by CS and borosilicate sphere (BS) tips as well as the surface morphology of these two tips. CSs of six different sizes were used for preparing colloidal probes (CPs). Quantitative adhesion force measurements of CS−CM interfaces were performed by employing the prepared CPs in atomic force microscope (AFM) peak-force mode (PFM). The theoretical adhesion forces calculated by the Johnson-Kendall-Roberts (JKR) model were compared with the experimental results of our adhesion measurements. The JKR values are

DOI: 10.1021/acs.langmuir.8b03503
Langmuir 2019, 35, 7312−7321

much higher than the experimental values because of the fact that the JKR model considers only interactions between smooth surfaces at equilibrium. In addition, the calculated JKR values increase constantly as the size of the CS increases, whereas the experimental values increase initially and then start to drop. This is due to the sudden decrease in the contact area at the primary valleys when the CS becomes too large to reach the bottom of the primary valley on the CM surface, which is predicted by the proposed new contact model. The experimental adhesion−surface height plots follow the proposed adhesion−surface morphology correlation pattern, as the adhesion peak values always appear at the primary and secondary valleys on the CM surface. More experiments using cellulose materials with controlled surface roughness are required in order to build an accurate mathematical model for rough-to-rough surface interactions.

AUTHOR INFORMATION

Corresponding Authors

*E-mail: xiehui@hit.edu.cn.
*E-mail: pasi.kallio@tuni.fi.

ORCID

Yuli Lai: 0000-0001-8043-0155
Hui Xie: 0000-0003-4299-2776
Pasi Kallio: 0000-0001-6698-774X

Author Contributions

‖These authors contributed equally.

Notes

The authors declare no competing financial interest.

ACKNOWLEDGMENTS

This project was supported by BioRa, European Commission (grant number 612641), WoodBone Projects, Academy of Finland (grant number 290304), and the National Key Research and Development Program of China (grant number 2017YFA0207201). The authors thank Professor Zuobin Wang and his team, especially Yingmin Qu, of Changchun University of Science and Technology for the FIB and SEM technique support.

REFERENCES

(1) Nigmatullin, R.; Lovitt, R.; Wright, C.; Linder, M.; Nakari-Setälä, T.; Gama, M. Atomic force microscopy study of cellulose surface interaction controlled by cellulose binding domains. *Colloids Surf., B* **2004**, *35*, 125−135.

(2) Huber, T.; Müssig, J.; Curnow, O.; Pang, S.; Bickerton, S.; Staiger, M. P. A critical review of all-cellulose composites. *J. Mater. Sci.* **2012**, *47*, 1171−1186.

(3) Butt, H. J. Measuring electrostatic, van der Waals, and hydration forces in electrolyte solutions with an atomic force microscope. *Biophys. J.* **1991**, *60*, 1438−1444.

(4) Ducker, W. a.; Senden, T. J.; Pashley, R. M. Direct measurement of colloidal forces using an atomic force microscope. *Nature* **1991**, *353*, 239−241.

(5) Dörig, P.; Ossola, D.; Truong, A. M.; Graf, M.; Stauffer, F.; Vörös, J.; Zambelli, T. Exchangeable colloidal AFM probes for the quantification of irreversible and long-term interactions. *Biophys. J.* **2013**, *105*, 463−472.

(6) Zauscher, S.; Klingenberg, D. J. Friction between cellulose surfaces measured with colloidal probe microscopy. *Colloids Surf., A* **2001**, *178*, 213−229.

(7) Notley, S. M.; Chen, W.; Pelton, R. Extraordinary adhesion of phenylboronic acid derivatives of polyvinylamine to wet cellulose: A colloidal probe microscopy investigation. *Langmuir* **2009**, *25*, 6898−6904.

(8) Zauscher, S.; Klingenberg, D. J. Normal Forces between Cellulose Surfaces Measured with Colloidal Probe Microscopy. *J. Colloid Interface Sci.* **2000**, *229*, 497−510.

(9) Notley, S. M.; Wågberg, L. Morphology of modified regenerated model cellulose II surfaces studied by atomic force microscopy: Effect of carboxymethylation and heat treatment. *Biomacromolecules* **2005**, *6*, 1586−1591.

(10) Notley, S. M.; Pettersson, B.; Wa, L.; Wågberg, L. Direct Measurement of Attractive van der Waals' Forces between Regenerated Cellulose Surfaces in an Aqueous Environment. *J. Am. Chem. Soc.* **2004**, *126*, 13930−13931.

(11) Stiernstedt, J.; Nordgren, N.; Wågberg, L.; Brumer, H.; Gray, D. G.; Rutland, M. W. Friction and forces between cellulose model surfaces: a comparison. *J. Colloid Interface Sci.* **2006**, *303*, 117−23.

(12) Sczech, R.; Riegler, H. Molecularly smooth cellulose surfaces for adhesion studies. *J. Colloid Interface Sci.* **2006**, *301*, 376−385.

(13) Leporatti, S.; Sczech, R.; Riegler, H.; Bruzzano, S.; Storsberg, J.; Loth, F.; Jaeger, W.; Laschewsky, A.; Eichhorn, S.; Donath, E. Interaction forces between cellulose microspheres and ultrathin cellulose films monitored by colloidal probe microscopy - Effect of wet strength agents. *J. Colloid Interface Sci.* **2005**, *281*, 101−111.

(14) Rutland, M.; Carambassis, A.; Willing, G.; Neuman, R. Surface force measurements between cellulose surfaces using scanning probe microscopy. *Colloids Surf., A* **1997**, *123−124*, 369−374.

(15) Carambassis, A.; Rutland, M. W. Interactions of cellulose surfaces: effect of electrolyte. *Langmuir* **1999**, *15*, 5584−5590.

(16) Theander, K.; Pugh, R. J.; Rutland, M. W. Friction force measurements relevant to de-inking by means of atomic force microscope. *J. Colloid Interface Sci.* **2005**, *291*, 361−368.

(17) Stiernstedt, J.; Brumer, H.; Zhou, Q.; Teeri, T. T.; Rutland, M. W. Friction between cellulose surfaces and effect of xyloglucan adsorption. *Biomacromolecules* **2006**, *7*, 2147−2153.

(18) Bastidas, J. C.; Pawlak, J. J.; Venditti, R. a.; Heitmann, J. a.; Hubbe, M. a.; Kadla, J. F. A colloidal probe microscopy study of cellulose/gypsum interactions. *Mater. Charact.* **2008**, *59*, 144−150.

(19) Ma, H.; Winslow, C. J.; Logan, B. E. Spectral force analysis using atomic force microscopy reveals the importance of surface heterogeneity in bacterial and colloid adhesion to engineered surfaces. *Colloids Surf., B* **2008**, *62*, 232−237.

(20) Kakui, T.; Miyauchi, T.; Kamiya, H. Analysis of the action mechanism of polymer dispersant on dense ethanol alumina suspension using colloidal probe AFM. *J. Eur. Ceram. Soc.* **2005**, *25*, 655−661.

(21) Drelich, J.; Long, J.; Xu, Z.; Masliyah, J.; Nalaskowski, J.; Beauchamp, R.; Liu, Y. AFM colloidal forces measured between microscopic probes and flat substrates in nanoparticle suspensions. *J. Colloid Interface Sci.* **2006**, *301*, 511−522.

(22) Zhang, X.; Lu, Y.; Liu, E.; Yi, G.; Jia, J. Adhesion and friction studies of microspherepatterned surfaces in contact with atomic force microscopy colloidal probe. *Colloids Surf., A* **2012**, *401*, 90−96.

(23) Giesbers, M.; Kleijn, J. M.; Fleer, G. J.; Cohen Stuart, M. a. Forces between polymer-covered surfaces: A colloidal probe study. *Colloids Surf., A* **1998**, *142*, 343−353.

(24) Horvath, E.; Lindström, T. The influence of colloidal interactions on fiber network strength. *J. Colloid Interface Sci.* **2007**, *309*, 511−517.

(25) Lidenmark, C.; Pettersson, T.; Karlsson, O. J.; Notley, S. M.; Norgren, M.; Hakan, E. The adhesive behavior of extracted latex polymers towards silicon oxide and cellulose. *Int. J. Adhes. Adhes.* **2013**, *44*, 250−258.

(26) Radtchenko, I. L.; Papastavrou, G.; Borkovec, M. Direct Force Measurements between Cellulose Surfaces and Colloidal Silica Particles. *Biomacromolecules* **2005**, *6*, 3057−3066.

(27) Gourianova, S.; Willenbacher, N.; Kutschera, M. Chemical force microscopy study of adhesive properties of polypropylene films: influence of surface polarity and medium. *Langmuir* **2005**, *21*, 5429−5438.

DOI: 10.1021/acs.langmuir.8b03503
Langmuir 2019, 35, 7312−7321

(28) Willing, G. a.; Ibrahim, T. H.; Etzler, F. M.; Neuman, R. D. New Approach to the Study of Particle and Surface Adhesion Using Atomic Force Microscopy. *J. Colloid Interface Sci.* **2000**, *226*, 185−188.
(29) Reynaud, C.; Sommer, F.; Quet, C.; Bounia, N. E.; Duc, T. M. Quantitative determination of Young's modulus on a biphase polymer system using atomic force microscopy. *Surf. Interface Anal.* **2000**, *30*, 185−189.
(30) Shen, Y.; Nakajima, M.; Kojima, S.; Homma, M.; Kojima, M.; Fukuda, T. Single cell adhesion force measurement for cell viability identification using an AFM cantilever-based micro putter. *Meas. Sci. Technol.* **2011**, *22*, 115802.
(31) Shen, Y.; Nakajima, M.; Ahmad, M. R.; Kojima, S.; Homma, M.; Fukuda, T. Effect of ambient humidity on the strength of the adhesion force of single yeast cell inside environmental-SEM. *Ultramicroscopy* **2011**, *111*, 1176−1183.
(32) Shen, Y.; Nakajima, M.; Kojima, S.; Homma, M.; Fukuda, T. Study of the time effect on the strength of cell−cell adhesion force by a novel nano-picker. *Biochem. Biophys. Res. Commun.* **2011**, *409*, 160−165.
(33) Pittenger, B.; Erina, N.; Su, C.. Mechanical Property Mapping at the Nanoscale Using PeakForce QNM Scanning Probe Technique. In *Nanomechanical Analysis of High Performance Materials: Solid Mechanics and Its Applications*; Tiwari, A., Ed.; Springer: 2014; Vol. *203*, pp 31−51.
(34) Martínez, L.; Tello, M.; Díaz, M.; Román, E.; Garcia, R.; Huttel, Y. Aspect-ratio and lateralresolution enhancement in force microscopy by attaching nanoclusters generated by an ion cluster source at the end of a silicon tip. *Rev. Sci. Instrum.* **2011**, *82*, 023710.
(35) Kumar, A.; Staedler, T.; Jiang, X. Role of relative size of asperities and adhering particles on the adhesion force. *J. Colloid Interface Sci.* **2013**, *409*, 211−218.
(36) Xie, H.; Hussain, D.; Yang, F.; Sun, L. Development of Three-Dimensional Atomic Force Microscope for Sidewall Structures Imaging with Controllable Scanning Density. *IEEE/ASME Trans. Mechatron.* **2015**, *21*, 316−328.
(37) Zhang, H.; Hussai, D.; Meng, X.; Song, J.; Xie, H. Calibration of Atomic Force Microscope Probes Using a Pneumatic Micro-manipulation System. *2017 International Conference on Manipulation, Automation and Robotics at Small Scales (MARSS)*; Montreal, QC, Canada, 2017; pp 1−6.
(38) Xie, H.; Zhang, H.; Song, J.; Meng, X.; Wen, Y.; Sun, L. High-Precision Automated Micromanipulation and Adhesive Microbonding with Cantilevered Micropipette Probes in the Dynamic Probing Mode. *IEEE/ASME Transactions on Mechatronics* **2018**, *23*, 1425−1435.
(39) Cleveland, J. P.; Manne, S.; Bocek, D.; Hansma, P. K. A nondestructive method for determining the spring constant of cantilevers for scanning force microscopy. *Rev. Sci. Instrum.* **1993**, *64*, 403−405.
(40) Quillin, D. T.; Caulfield, D. F.; Koutsky, J. A. Materials interactions relevant to recycling of wood-based materials: Proceedings of Materials Research Society symposium. *Proc. Mater. Res. Soc. Symp.* **1992**, *266*, 113−126.
(41) Nordgren, N.; Lo, H.; Hult, A.; Malmstro, E.; Rutland, M. W. Adhesion Dynamics for Cellulose Nanocomposites. *ACS Appl. Mater. Interfaces* **2009**, *1* (2), 2098−2103.

DOI: 10.1021/acs.langmuir.8b03503
Langmuir 2019, 35, 7312−7321